Chalcogen Bonding of Two Ligands to Hypervalent YF_4 (Y=S, Se, Te, Po)

Wiktor Zierkiewicz,*[1] Rafał Wysokiński,[1] Mariusz Michalczyk, [1] and Steve Scheiner*[2]

[1] Faculty of Chemistry, Wrocław University of Science and Technology, Wybrzeże Wyspiańskiego 27, 50-370 Wrocław, Poland

[2] Department of Chemistry and Biochemistry, Utah State University Logan, Utah 84322-0300, United States

*Correspondence to: wiktor.zierkiewicz@pwr.edu.pl; steve.scheiner@usu.edu

Abstract

The ability of two NH_3 ligands to engage in simultaneous chalcogen bonds to a hypervalent YF_4 molecule, with Y=S, Se, Te, Po, is assessed via quantum calculations. The complex can take on one of two different geometries. The *cis* structure places the two ligands adjacent to one another in a pseudo-octahedral geometry, held there by a pair of σ-hole chalcogen bonds. The bases can also lie nearly opposite one another, in a distorted octahedron containing one π-hole and one strained σ-hole bond. The *cis* geometry is favored for Y=S, while Te, and Po tend toward the *trans* structure; they are nearly equally stable for Se. In either case, the binding energy rises rapidly with the size of the Y atom, exceeding 30 kcal/mol for PoF_4.

Keywords: σ-hole; π-hole; AIM; frequencies

1. Introduction

Current knowledge about noncovalent interactions derives from centuries of continuous studies dating back to 1873 and the groundbreaking work of van der Waals concerning real gases[1]. Nowadays the role of intermolecular noncovalent interactions, even though they are weaker and less directional than covalent bonds, is no longer in question. Noncovalent interactions are major factors in the formation of molecular clusters, crystal engineering, drug chemistry, molecular recognition, material design, and organic synthesis.[2-17] As one important example, the chalcogen bond (commonly abbreviated as YB or ChB)[18] is defined as the attractive interaction between a positively polarized chalcogen atom and a nucleophile. Among its potential applications are ligand-protein contacts [16,19-22], synthesis of organic compounds[2,23-26] and crystal structure frameworks.[13,27-31] Chalcogen bonding is one of several subclasses of σ-hole theory[32-40] which is based on the local depletion of electron density on the outermost portion of a chalcogen atom which is involved in an intramolecular covalent bond with an electron-withdrawing group. The resulting partially positively charged area on this chalcogen can attract an approaching Lewis base. After its introduction as a factor in halogen bonding[41] this notion was successfully extended to other groups of elements, including chalcogen.[35,42,43] The intensity of σ-holes on the chalcogens grows in the O < S < Se < Te order, along with increasing atomic polarizability and diminishing electronegativity.[26] This Coulombic attraction is supplemented by orbital interactions such as charge transfer and dispersion terms which are also important components.[44] The positive area is not limited to a σ-hole, but can in certain cases occur above a planar molecule, as in triel bonded systems,[45,46] where it is commonly referred to as a π-hole.[47,48]

Various aspects of chalcogen bonds have been discussed in recent years. For instance, it was found that appended hydrogen and lithium bonds can enhance the strength of chalcogen bonds in $NCH\cdots(OCY)_{n=2-5}$ and $NCLi\cdots(OCY)_{n=2-5}$ clusters (Y=S, Se) by increasing the amount of $LP(O)\rightarrow\sigma_{C\text{-}X}$ orbital transfer and σ-hole potential on the chalcogen atom.[49] Chalcogen bonding motifs are frequently found in biologically important structures, for example in Ebselen (a synthetic organoselenium drug molecule) where the short Se···O contacts may be responsible for its biological activity.[18,50] The diselenide moiety was very recently discovered in bis(*o*-anilinium)diselenide salts where the chalcogen bonded network stabilizes the crystal structure due to the presence of two σ-holes along the covalent bonds in which each Se atom is involved.[29] Lastly, Kar *et al.* found that chalcogen-rich transition metal complexes (trimetallic clusters, with Nb and Ta atoms) which can be exploited in metalloenzymes studies, are stabilized by S-S and Se-Se chalcogen bridges.[51]

Despite a substantial number of insights that may be gleaned from the recent literature concerning chalcogen bond nature and functionality,[13,16,19,52,53] there are still a number of fundamental questions. In the first place, the vast majority of study has concerned the presence of a single such bond to a given chalcogen atom. There is no reason to think that each chalcogen atom has a strict limit of one noncovalent bond, and indeed the crystallographic literature is replete with examples of multiple chalcogen bonds. It is thus important to consider the

possibility of two such bonds, and how they might influence one another, as well as the geometry of the resulting complex. A second issue has to do with the coordination of the central chalcogen atom. The majority of past work has considered divalent chalcogen bonds of the type YR_2 where Y represents a chalcogen atom, and R a general substituent. Yet chalcogen atoms are known to commonly involve themselves in other coordinations, most notably YR_4. These additional substituents are likely to introduce a higher degree of steric crowding, making it more difficult for an incoming base, or bases, to approach within noncovalent bonding proximity to the Y atom. Taking S as an example, divalent sulfur in SF_2 was examined in dimeric complexes with diazines and amine derivatives and other systems.[54-56] Although hypervalent SF_4 is well known and characterized [57], it has been the subject of far fewer investigations with respect to its ability to engage in a chalcogen bond.[58-60] And in neither case is there available any information about their capacity with respect to more than one such bond. There is even less information in the literature concerning the atoms below S in the periodic table.

It is the goal of the present communication to cover the present gaps in our understanding of this problem. Hypervalent YF_4 molecules are allowed to interact with a pair of Lewis bases to determine firstly whether two chalcogen bonds are even possible for this crowded species. The implications of the size of the chalcogen atom Y on this question are addressed by comparing the full range of chalcogen atoms from S to Po. (This work constitutes the first examination of the capacity of the Po atom to engage in a chalcogen bond of any sort.) There is more than one possibility regarding the overall geometry of a complex containing two chalcogen bonds, so the relative stabilities and properties of all such structures are compared. The work also considers how the dual chalcogen bond formation affects the internal geometry and spectral characteristics of the central YF_4 molecule.

2. COMPUTATIONAL METHODS AND SYSTEMS

Tetrasubstituted YF_4, with Y= S, Se, Te, and Po, was taken as a model chalcogen-containing hypervalent Lewis acid. Each such molecule contains four Y-F bonds, and one Y lone electron pair. The range of chalcogen atoms permits determination of how atom size and polarizability affect the properties of the binding. The highly electronegative F atoms maximize the ability of these Y atoms to engage in chalcogen bonds with an incoming base. NH_3 was chosen as the Lewis base for a number of reasons. Its simplicity minimizes complicating secondary effects, and its high basicity optimizes its ability to interact with a given Lewis acid. In addition, it is the most common base that has been studied in works of this sort which facilitates comparison with past results.

Geometries of monomers and complexes were optimized at the MP2/aug-cc-pVDZ level of theory.[61,62] Relativistic effects were incorporated for the Te and Po atoms by use of the corresponding pseudopotentials from the EMSL library.[63] Two other levels of theory: BLYP-D3/def2TZVPP[64,65] and CCSD(T)/aug-cc-pVDZ[66-68] were applied in order to assess the accuracy of energetics. Harmonic frequency calculations verified optimized structures as true energy minima (no imaginary frequencies) and facilitated comparisons of infrared spectra. To provide

unambiguous assignments of the spectra, a normal mode analysis was carried out and the potential energy distribution (PED) was calculated at the MP2/aug-cc-pVDZ level. The non-redundant sets of symmetrized internal coordinates for isolated monomers as well as complexes were defined, as recommended by Pulay et al.,[69] and are available in Supplementary Information. The procedure for normal coordinate analysis was described previously,[70,71] and calculations were performed using the Balga program.[72] Interaction (E_{int}) and binding (E_b) energies were calculated as the differences between the electronic energy of the complex and sum of the electronic energies of three monomers in the geometry within the complex (E_{int})[73] or in their isolated form (E_b). The difference between E_{int} and E_b is the deformation energy (E_{def}) which embodies the energetic cost of distortion of the monomers from their fully optimized geometry to that adopted within the complex. These quantities were corrected for basis set superposition error (BSSE) via the counterpoise protocol.[74] Calculations were carried out using the Gaussian 09 suite of programs.[75] Molecular electrostatic potential (MEP) analysis applied to visualize and quantify extrema on the molecular surface was performed using the WFA-SAS and MultiWFN programs.[76-78] Noncovalent index (NCI)[79] analysis embedded in MultiWFN software was employed to identify the interaction regions between monomers held together by noncovalent forces and assess their magnitude. QTAIM analysis of wavefunctions obtained for MP2 optimized geometries quantified the topology of the electron density.[80] The CSD (Cambridge Structural Database)[81] was explored to identify experimental crystal structures confirming the sorts of interactions examined here.

3. Results

3.1. Monomers

The optimized structure of all isolated YF_4 monomers (Y = S, Se, Te, Po) was of see-saw type as illustrated in Fig 1, i.e. a trigonal bipyramid with one equatorial position occupied by a Y lone pair. The remaining two equatorial F atoms are labeled F_e and F_a indicates the two axial F atoms. The details of the geometry of each are contained in Table S1, where it may be seen that the r(Y-F_a) bond lengths are longer than r(Y-F_e), and this difference becomes smaller as the Y atom grows in size. Were all four F atoms to lie in a common plane, the sum of the four θ(F_a-Y-F_e) angles would be 360°, so the deviation of this sum from that value, serves as a measure of the nonplanarity. This quantity, reported in the last column of Table S1 indicates SF_4 is the least nonplanar with a sum of 350°, and TeF_4 the most at 339°.

All of the YF_4 monomers have a very similar molecular electrostatic potential (MEP), and that of SF_4 is presented in Fig 2 as an example. One can see two positive regions (σ-holes), each lying along the extension of a Y-F_e bond. The magnitudes ($V_{s,max}$) of these holes are 41.7, 51.2, 59.2, and 76.3 kcal/mol, for Y=S, Se, Te, Po, respectively so clearly increases along with the size of the Y atom.

Table S2 lists selected harmonic frequencies and IR intensities of isolated YF_4 monomers, which are presented graphically in Fig S1. As a first observation, both symmetric and antisymmetric stretching vibrations of the equatorial Y-F bonds appear at higher frequencies than

for their axial counterparts. Secondly, all frequencies shift to the red as the Y atom grows larger, and the intensities diminish in the same order. All these vibrations are formally infrared active, although some of them are of very low intensity. For example, it is doubtful that the $\nu_s(Y\text{-}F_a)$, twist($Y\text{-}F_a$), or out-of-plane motions could be detected, due to very small intensities.

3.2. Complexes

3.2.1. Equilibrium Geometries and Energies

YF_4 engages in two sorts of complexes when paired with two NH_3 molecules, both of which are illustrated graphically in Fig 3. In the first geometry, each of the two bases approaches Y toward a σ-hole along a $Y\text{-}F_e$ bond extension. The entire structure takes on an octahedral shape, albeit a distorted one, and is termed *cis* as the two bases lie adjacent to one another. The second complex involves a distortion of the YF_4 molecule from a see-saw to a nearly planar square shape, with roughly equivalent F atoms. One NH_3 approaches from a direction perpendicular to the YF_4 plane, toward a π-hole that exists above the Y, so is considered a π-hole bond. The second NH_3 sits closer to the YF_4 pseudo-plane, roughly opposite one of the F atoms in a distorted σ-hole geometry. As the two bases lie approximately opposite one another, this second structure is referred to as *trans*.

The two sorts of structures are comparable in energy. Indeed the choice as to the more stable depends upon the Y atom. The electronic *energies* in Table 1 indicate that *cis* is favored for SF_4, but *trans* is preferred for both TeF_4 and PoF_4, with SeF_4 showing no difference. A similar pattern is seen in the free energies, although SeF_4 shows a distinct preference for *trans* in this property.

Focusing first on the structural details of the *cis* geometries, the two NH_3 ligands are not equivalently disposed, as one lies closer to Y than does the other. This distinction is trivial for Y=S and Se, but is more noticeable for Te and Po, as shown in Table 2. Nor is this distinction an artifact of any particular basis set, as optimization with other sets reproduced this asymmetry. Formation of the complex elongates all of the Y-F bonds, more so for $Y\text{-}F_a$. The latter fact is a bit surprising as it is the $Y\text{-}F_e$ σ-hole that the two NH_3 bases occupy. The angles listed in Table 2 display regular patterns. The angle separating the two equatorial $Y\text{-}F_e$ or axial $Y\text{-}F_a$ bonds becomes smaller as Y grows larger. At the same time, the separation between the two NH_3 bases increases.

The possibility of an intermolecular HB between a NH of NH_3 and one of the F atoms is explored in the last column of Table 2 which displays the shortest such distance. It may be noted that there is a clear distinction between the lighter Y atoms for which this r(H··F) exceeds 2.9 Å and the two heavier Y for which it is less than 2.6 Å. It is perhaps this supplementary HB which pulls one NH_3 in closer than the other in the latter TeF_4 and PoF_4 complexes. In order to further explore this possibility, the two NH_3 bases were replaced by linear N≡CH which precludes such an intermolecular HB. Optimization led to equal R(Te··N) distances when these bases were added to TeF_4.

NCI analysis permits a graphical view of the various interactions, repulsive and attractive alike. The relevant diagrams are presented in Fig S2 where red and brown colors represent repulsive forces, and green and blue indicate attractions. The suspected intermolecular NH··F

HBs in the Te and Po complexes are confirmed by the diagrams on the left side of this figure which refer to the *cis* complexes.

Turning next to the *trans* structures, it is clear from Table 3 that the binding of the two NH_3 ligands is quite different. One of them, the one that occupies a π-site, lies much closer to the Y than does the other, with a difference of as much as 1.2 Å. The R(Y··N) distance of this π base is quite short, between 1.87 and 2.28 Å, while the σ base is something on the order of 3 Å from Y. Note also that the former distance becomes longer as Y grows larger, but the latter behaves in the opposite way. The geometry of the *trans* complexes may be understood in the context of the electronic structure of the central YF_4. As this molecule alters its geometry toward a square pyramid to form a π-hole complex with one NH_3, the Y atom retains a doubly occupied lone pair which lies directly opposite this NH_3, as shown in Fig S3. This lone pair obstructs the path of a second NH_3 toward the Y, on both steric and electrostatic grounds, forcing it to bend away from the C_4 axis of YF_4. As a manifestation of the lone pair electrons' effect on the MEP, $V_{s,max}$ in the region where it occurs is smaller by 20-60 kcal/mol than the same maximum in the opposite direction, where NH_3 engages in a π-hole interaction.

All four of the r(YF) bond lengths are listed in the next column of Table 3 where it may be seen that these are all longer than the comparable bonds in the *cis* complexes, with the exception of PoF_4 where there is little difference between *trans* and r(YF_a). The sum of four θ(F-Y-F) angles would be 360° were the YF_4 unit fully planar so the deviation in this sum from 360° is a measure of nonplanarity, which is greatest for Te and Po. The angle separating the two NH_3 molecules is contained in the last column and is highly nonlinear, lying in the 129°-140° range.

The binding energies (E_b) of the two NH_3 molecules to YF_4 are collected in the left half of Table 4. As an initial observation, all three levels of theory, including MP2, BLYP-D3 and CCSD(T), provide very similar quantities, with some overestimation noted in DFT for certain complexes. All methods agree that the binding energies increase rapidly as the Y atom grows in size. This quantity can be as small as 2.8 kcal/mol for Y=S but reach up to 35 kcal/mol for PoF_4. It is interesting to note that the *cis* structures are more strongly bound than *trans* for the two lighter Y atoms, but the reverse occurs for Te and Po, even if the differences are small.

The binding energies take as their starting point the energies of the three units in their fully optimized geometries. Another related energetic quantity known as the interaction energy E_{int} starts each monomer in the structure it attains within the full complex. Since E_b involves first a destabilizing deformation of each monomer, it is of course less negative than E_{int}, which is reflected in comparison of the left and right sides of Table 4. The trends noted for E_b of the *cis* structures remain largely intact for E_{int}, both growing with larger size of Y. Their difference, representing the monomer strain energies, are not very large less than 7 kcal/mol. But the deformation energy is far larger for the *trans* structures, making E_{int} much more negative than E_b. This deformation energy is largest for S, amounting to 48 kcal/mol, and smallest for Po, still as large as 18 kcal/mol. Whereas the binding energy of the *trans* complexes varied in the 3-35 kcal/mol range, E_{int} is much more exothermic 47-52 kcal/mol. Moreover, there is little sensitivity of E_{int} to the identity of the central Y atom. The numerical values of the deformation

energies of the individual monomers are listed in Table S3, along with the values of the MEP maxima within the distorted YF_4 units.

3.2.2. QTAIM Analysis

A useful window into the nature and strength of noncovalent bonding is offered by AIM analysis of the topology of the electron density.[82,83] The molecular diagrams are displayed in Fig. 4 where bond paths are indicated by broken lines, with the corresponding bond critical point (BCP) as a small green dot. The diagrams confirm that there are no secondary interactions in the *cis* structures, other than the expected Y··N bonds. The values of the density at these points generally increase along with the size of the Y atom (although the two Y··N bonds become more asymmetric as well). This trend agrees with the energetic data in Table 4. The *trans* complexes suggest a very strong Y··N bond to the closer NH_3 in the π-hole, with ρ_{BCP} diminishing from 0.160 for S down to half that quantity for the largest Po. These π-bonds thus appear to be much stronger than the pair of chalcogen bonds in the *cis* complexes. On the other hand, the other Y··N' bond to the more distant NH_3 is considerably weaker, consistent with its much longer interatomic distance. These diagrams of the *trans* structures also show evidence of NH··F HBs for Y=S and Se, even if these bonds appear weaker than the central Y··N. The values of the Laplacian of the electron density, a measure of the concentration of electron density in the interatomic space, are positive for all trimers (table S4) which suggests depletion of electron density typically found for unshared interactions.[84]

Data of a similar nature were collected by Del Bene *et al.*[85] where C···S chalcogen bonds were studied in SC···SHX complexes (X=NO_2, NC, F, Cl, CN, CCH, and NH_2). At long C···S distances $\nabla^2\rho$ was positive, but reversed sign for shorter contacts, which was interpreted as a differentiation between traditional, noncovalent chalcogen bonds and stronger, shared ones. For their strongest, but still noncovalent, chalcogen bonds ρ was around 0.1 au, comparable to the π-bonds here, while shared bonds hovered around 0.2 au. With respect to the SF_4 molecule, its complex with pyridine[86] exhibited a S··N ρ at BCP of 0.037 au, similar to values obtained in this paper for the two S···N interactions in *cis* $(H_3N)_2\cdots SF_4$.

3.2.3. Vibrational Spectra

The calculated harmonic frequencies and intensities of the *cis* and *trans* geometries are compiled in Tables S5 and S6, respectively. Focusing first on the intermolecular stretching modes, the near equivalence of the two σ-hole Y··N bonds in the *cis* structures lead to both symmetric and asymmetric Y··N stretches. The former are of higher frequency and lie in the 141-262 cm^{-1} range; the latter 80-203 cm^{-1}. Their intensities vary from very small for the lighter Y atoms, but are larger for Te and Po, although still less than 300 km/mol. The substantial difference between the two NH_3 ligands in the *trans* structures uncouple the two Y··N stretches. The frequency involving the closer N atom exceed 400 cm^{-1}, and the longer Y··N' stretch lies in the 116-187 cm^{-1} range. The intensities of these bands are all less than 43 km/mol. One might expect some correlation between the intermolecular stretching frequency and the intensity of the σ-hole that draws in the base. For example, a tight linear relationship was shown recently in the pnicogen bonded $ZF_2C_6H_5$ (Z = P, As, Sb, Bi) complexes with an ammonia ligand.[87] In this

case, when ν_s(N···Y) was related to $V_{s,max}$ (of the *cis* complex with the closer ligand removed), the correlation coefficient of Fig S4 is only 0.83.

The changes that the Y-F stretches undergo upon formation of the *cis* and *trans* complexes are reported in Tables 5 and 6, respectively. It may be noted first that the attachment of a pair of NH_3 molecules diminishes the frequencies of the Y-F stretches, both symmetric and asymmetric, and whether *cis* or *trans* These red shifts lie in the general range of 36 to 71 cm^{-1} for the *cis* structures, and are generally of slightly larger magnitude for the antisymmetric stretches, but do not distinguish in an obvious way between axial and equatorial F atoms. Nor is there much sensitivity of these shifts to the nature of the Y atom. While most of these modes gain in intensity upon complexation, there is one major exception in that the ν_a(Y-F_a) mode drops by nearly 100 km/mol. Of course, there is no longer a distinction between equatorial and axial F atoms in the *trans* complexes, and the red shifts of the Y-F stretches in Table 6 are generally of larger magnitude than in their *cis* analogues. Unlike the *cis* case, there is a general lowering trend in these red shifts as the Y atom grows in size.

3.2.4. Survey of Crystal Data

It is instructive to compare the calculated data obtained here with any experimental geometries available from past crystal diffraction studies. A search of the CSD (Cambridge Structural Database)[81]was directed toward any interactions between a hypervalent Y atom (Y=S, Se, Te, Po) covalently bonded to one or more halogen atoms and associated with one or two ligands linked through N or S atoms. These conditions yielded a total of 15 structures with one such N or S ligand. In addition, 25 structures were identified with two ligands, of which 2 involved N atoms (both *cis* arranged) and 23 with S ligands (13 *cis* and 10 *trans*). Several examples[88-91] are displayed in Fig 5 for the particular case of Y=Te. HUCCEN and LUDJUP place the central atom in an octahedral arrangement, surrounded by four Cl ligands, and axial placement of the two S-containing ligands, reminiscent of our calculated *trans* structures. As examples of *cis* geometries, EFIVUL and HUQNAJ position the N-containing ligands adjacent to one another. With respect to some of the finer points of the geometries, *trans* HUCCEN displays an asymmetry between the two R(Te··S) distances, similar to the calculated Te geometries, while these distances are equivalent in LUDJUP. The calculated *cis* structure symmetries differed depending upon Y, with lighter Y displaying equivalence that fades for heavier Y. The particular *cis* structures EFIVUL and HUQNAJ are both symmetric, or nearly so. One might conclude then that the degree of asymmetry between the two ligands is a delicate one, influenced by size of Y atom, nature of ligand, and other environmental effects introduced within the context of a crystal.

4. Discussion

There has been little prior consideration of more than one noncovalent interaction to a central atom[92]. One work[93] considered the possibility of two simultaneous noncovalent bonds to a single tetrel atom (T) of TF_4. As in the present work dealing with chalcogen bonds, there were two possibilities for the geometry of the complex. The tetrahedral molecule could adopt a square planar geometry which provides a pair of π-holes which can each attract a nucleophile, which are

trans to one another. The alternate possibility was also octahedral in overall structure, but had the two bases *cis* to one another as they interacted with two σ-holes. While the former involved a stronger set of interactions, it also was encumbered by a larger distortion energy, making the *cis* structure somewhat more stable.

As indicated earlier, there is already available substantial information which has accumulated [94-101] in the literature dealing with a single chalcogen bond to a divalent Y atom. The results here are consistent with the prior data in a number of ways. In the first place, there is a tendency for each incoming nucleophile to approach along the extension of a F-Y bond where a σ-hole is present. Chalcogen bonds tend to strengthen as the Y atom grows in size. This bond strengthening, and its accompanying push toward a shorter bond, opposes the natural trend of a longer distance that would arise from a larger Y atom. As a result, the R(Y··N) distance does not change in a simple, regular fashion. The internal r(YF) bond lengths of the central unit are elongated by the chalcogen bond, and their corresponding stretching frequencies shifted to the red.

With respect to a hypervalent species such as YF_4, the available information is a bit sparser and limited to a single chalcogen bond, but worth comparison nonetheless. A single NH_3 base [102] approaches the YF_4 subunit along a σ-hole opposite one of the two equatorial F atoms, reminiscent of the geometry of the *cis* structure here. The bond strength increased regularly from 6.6 kcal/mol for SF_4 to 16.0 kcal/mol for TeF_4, while the R(Y··N) distance pattern was less regular. Adding methyl groups to the small NH_3 base enhanced the binding energy, as did its replacement by one of a set of heteroaromatic amines [103]. It was noted as well that induction energy was a major contributor to these chalcogen bonds. A tetravalent S atom was also studied in the context of an intramolecular chalcogen bond [104] where it was subject to a certain amount of strain. Despite this strain, and the alteration of the base atom from N to O, there was evidence of r(S-F) bond elongation, as noted here. Modification of the molecule enabled the formation of two S··O chalcogen bonds, suggesting there is a strong trend in this direction even in the face of intramolecular strain. A direct comparison was drawn between tetravalent SF_4 and SF_2, in connection with their ability to engage in a chalcogen bond with a π-electron donor [105]. The divalent species formed shorter and stronger chalcogen bonds in most cases, but there were exceptions as well. In either case, chalcogen bond formation engendered S-F bond elongations, and these Y··π bonds were highly dependent upon induction components. A very recent work [106] observed that the preference between two σ-holes on tetravalent S represents a balance between electrostatic and polarizability arguments.

There is some prior confirmation of our observation here that formation of a noncovalent bond is sufficient incentive for a molecule to undergo substantial deformation so as to maximize this interaction, mainly in the context of tetrel and pnicogen bonds [107,108] and that this distortion can influence the preference of an incoming base for one σ-hole over another [109]. In the context of hypervalent molecules, ZF_5, where Z represents a pnicogen atom, [110-111] takes on a trigonal bipyramid shape as a monomer, but then distorts into a square pyramid so as to accommodate an incoming nucleophile, at significant cost in terms of deformation energy. A hypervalent XF_5

molecule (X=halogen) requires somewhat less deformation energy as it is already in the proper shape to accommodate a noncovalent bond.

There has been some earlier comparison of π-holes vs σ-holes in terms of the strength of their interaction [112-114]. Within the context of tetrel bonds, the π-holes lying above the plane of $R_2T{=}CH_2$ molecules (T=tetrel atom) present stronger interactions [115] than their σ-hole correlates in TR_4 molecules. When paired with borazine, similarly shaped molecules display a preference for π-hole interactions [116]. As in the case of tetrel bonds, the competition between the σ and π-holes of pnicogen atoms can be controlled by the deformation energies associated with each [87]. Aerogen (Ae=Kr,Xe) atoms within a $AeOF_2$ molecule favor [117] σ over π-holes.

5. Conclusions

There are two frameworks in which a YF_4 molecule can engage in two simultaneous chalcogen bonds with a pair of NH_3 bases. In the first, the two bases occupy adjacent positions along Y σ-holes in a modified octahedral geometry. An alternative to this *cis* structure is a *trans* geometry in which the YF_4 molecule deforms from a see-saw into a nearly square planar conformation. One NH_3 lies along a π-hole above the YF_4 pseudoplane while the other lies roughly along a σ-hole, and is much more distant from the central Y. The latter conformation is subject to a high deformation energy in order to achieve this nearly planar structure, but on the other hand benefits from a much stronger interaction between the central unit and the bases. When these two opposing effects are combined, the two geometries have comparable stabilities. The *cis* structure is preferred over the *trans* for SF_4, but it is the *trans* that is the more stable for the larger Te and Po atoms; *cis* and *trans* are equally stable for Se. The binding energies are quite sensitive to the size of the chalcogen atom, ranging from 11 kcal/mol for SF_4 up to more than 30 kcal/mol for Y=Po. Complexation of either sort induces stretches of the Y-F bonds and red shifts in their stretching frequencies.

Conflicts of interest

There are no conflicts to declare.

Acknowledgements

This work was financed in part by a statutory activity subsidy from the Polish Ministry of Science and Higher Education for the Faculty of Chemistry of Wroclaw University of Science and Technology. A generous computer time from the Wroclaw Supercomputer and Networking Center is acknowledged.

References

1. Van Der Waals, J. D. Over de Continuiteit Van der Gas-en Vloeistoftoestand 1873.
2. Mahmudov, K. T.; Kopylovich, M. N.; Guedes da Silva, M. F. C.; Pombeiro, A. J. L. Coordin Chem Rev 2017, 345, 54-72.
3. Wheeler, S. E.; Seguin, T. J.; Guan, Y.; Doney, A. C. Accounts Chem Res 2016, 49, 1061-1069.
4. Beno, B. R.; Yeung, K. S.; Bartberger, M. D.; Pennington, L. D.; Meanwell, N. A. Journal of Medicinal Chemistry 2015, 58, 4383-4438.
5. Konu, J.; Chivers, T.; Tuononen, H. M. Chemistry - A European Journal 2010, 16, 12977-12987.
6. Chivers, T.; Konu, J. Angewandte Chemie - International Edition 2009, 48, 3025-3027.
7. Desiraju, G. R. Angewandte Chemie - International Edition 2007, 46, 8342-8356.
8. Werz, D. B.; Gleiter, R.; Rominger, F. J Am Chem Soc 2002, 124, 10638-10639.
9. Etter, M. C. Accounts Chem Res 1990, 23, 120-126.
10. Desiraju, G. R. Angewandte Chemie International Edition in English 1995, 34, 2311-2327.
11. Zhang, Y.; Wang, W. Z.; Wang, Y. B. Comput Theor Chem 2019, 1147, 8-12.
12. Mahmudov, K. T.; Gurbanov, A. V.; Guseinov, F. I.; da Silva, M. F. C. G. Coordin Chem Rev 2019, 387, 32-46.
13. Chen, L.; Xiang, J.; Zhao, Y.; Yan, Q. J Am Chem Soc 2019, 141, 3316-3316.
14. Zhang, T. X.; Wang, L. G.; Zhu, J. J.; Liu, J. Y.; Guo, S. J. J Nanoelectron Optoe 2019, 14, 227-231.
15. Verma, A.; Tomar, K.; Bharadwaj, P. K. Cryst Growth Des 2019, 19, 369-375.
16. Borissov, A.; Marques, I.; Lim, J. Y. C.; Felix, V.; Smith, M. D.; Beer, P. D. J Am Chem Soc 2019, 141, 4119-4129.
17. Montaña, Á. M. Chemistryselect 2017, 2, 9094-9112.
18. Vogel, L.; Wonner, P.; Huber, S. M. Angew Chem Int Edit 2019, 58, 1880-1891.
19. Ams, M. R.; Trapp, N.; Schwab, A.; Milic, J. V.; Diederich, F. Chem-Eur J 2019, 25, 323-333.
20. Fischer, M.; Schmidtmann, M.; Beckhaus, R. Z Anorg Allg Chem 2019, 645, 595-604.
21. Kriz, K.; Fanfrlik, J.; Lepsik, M. Chemphyschem 2018, 19, 2540-2548.
22. Karshikoff, A. Non-Covalent Interactions in Proteins; IMPERIAL COLLEGE PRESS., 2006.
23. Polgar, A. M.; Corrigan, J. F. Phys Sci Rev 2019, 4.
24. Pop, A.; Silvestru, C.; Silvestru, A. Phys Sci Rev 2019, 4.
25. Wang, S. T.; Yan, C. X.; Shang, J. H.; Wang, W. B.; Yuan, C. S.; Zhang, H. L.; Shao, X. F. Angew Chem Int Edit 2019, 58, 3819-3823.
26. Mahmudov, K. T.; Kopylovich, M. N.; Guedes da Silva, M. F. C.; Pombeiro, A. J. L. Dalton *trans* 2017, 46, 10121-10138.
27. Bartashevich, E.; Mukhitdinova, S.; Yushina, I.; Tsirelson, V. Acta Crystallogr B 2019, 75.
28. Riel, A. M. S.; Jeannin, O.; Berryman, O. B.; Fourmigue, M. Acta Crystallogr B 2019, 75, 34-38.
29. Scilabra, P.; Murray, J. S.; Terraneo, G.; Resnati, G. Cryst Growth Des 2019, 19, 1149-1154.
30. Shestimerova, T. A.; Kuznetsov, A. N.; Shevelkov, A. V. Struct Chem 2019, 30, 443-450.
31. Tao, Y. W.; Zou, W. L.; Sethio, D.; Verma, N.; Qiu, Y.; Tian, C.; Cremer, D.; Kraka, E. J Chem Theory Comput 2019, 15, 1761-1776.

32. Clark, T.; Hennemann, M.; Murray, J. S.; Politzer, P. J Mol Model 2007, 13, 291-296.
33. Murray, J. S.; Lane, P.; Clark, T.; Politzer, P. J Mol Model 2007, 13, 1033-1038.
34. Murray, J. S.; Lane, P.; Politzer, P. Int J Quantum Chem 2007, 107, 2286-2292.
35. Murray, J. S.; Lane, P.; Politzer, P. J Mol Model 2009, 15, 723-729.
36. Murray, J. S.; Lane, P.; Clark, T.; Riley, K. E.; Politzer, P. J Mol Model 2012, 18, 541-548.
37. Murray, J. S.; Resnati, G.; Politzer, P. Faraday Discussions 2017, 203, 113-130.
38. Politzer, P.; Murray, J. S.; Clark, T.; Resnati, G. Phys Chem Chem Phys 2017, 19, 32166-32178.
39. Clark, T.; Murray, J. S.; Politzer, P. Phys Chem Chem Phys 2018, 20, 30076-30082.
40. Politzer, P.; Murray, J. S. J Comput Chem 2018, 39, 464-471.
41. Desiraju, G. R.; Shing Ho, P.; Kloo, L.; Legon, A. C.; Marquardt, R.; Metrangolo, P.; Politzer, P.; Resnati, G.; Rissanen, K. Pure and Applied Chemistry 2013, 85, 1711-1713.
42. Politzer, P.; Murray, J. S.; Concha, M. C. J Mol Model 2008, 14, 659-665.
43. Pandiyan, B. V.; Deepa, P.; Kolandaivel, P. Mol Phys 2016, 114, 3629-3642.
44. Esrafili, M. D.; Mousavian, P.; Mohammadian-Sabet, F. Mol Phys 2019, 117, 58-66.
45. Michalczyk, M.; Zierkiewicz, W.; Scheiner, S. Chemphyschem 2018, 19, 3122-3133.
46. Chi, Z.; Dong, W.; Li, Q.; Yang, X.; Scheiner, S.; Liu, S. Int J Quantum Chem 2019, 119, e25867.
47. Politzer, P.; Murray, J. S. Crystals 2019, 9.
48. Bauza, A.; Frontera, A.; Mooibroek, T. J. Cryst Growth Des 2016, 16, 5520-5524.
49. Esrafili, M. D.; Mousavian, P.; Mohammadian-Sabet, F. Mol Phys 2019, 117, 726-733.
50. Thomas, S. P.; Satheeshkumar, K.; Mugesh, G.; Guru Row, T. N. Chemistry – A European Journal 2015, 21, 6793-6800.
51. Kar, S.; Bairagi, S.; Saha, K.; Raghavendra, B.; Ghosh, S. Dalton T 2019, 48, 4203-4210.
52. Gougoula, E.; Medcraft, C.; Alkorta, I.; Walker, N. R.; Legon, A. C. Journal of Chemical Physics 2019, 150.
53. Ben Aissa, M. A.; Hassen, S.; Arfaoui, Y. Int J Quantum Chem 2019, 119.
54. Su, H.; Wu, H.; Wang, H.; Wang, H. Y.; Ni, Y. X.; Lu, Y. X.; Zhu, Z. D. J Mol Struct 2019, 1188, 62-68.
55. Zierkiewicz, W.; Fanfrlik, J.; Michalczyk, M.; Michalska, D.; Hobza, P. Chem Phys 2018, 500, 37-44.
56. Zierkiewicz, W.; Michalczyk, M.; Bienko, D.; Michalska, D.; Zeegers-Huyskens, T. Int J Quantum Chem 2017, 117.
57. Levin, I. W.; Berney, C. V. Journal of Chemical Physics 1966, 44, 2557-&.
58. Nziko Vde, P.; Scheiner, S. J Phys Chem A 2015, 119, 5889-5897.
59. Vincent De Paul, N. N.; Scheiner, S. Journal of Physical Chemistry A 2014, 118, 10849-10856.
60. Chaudhary, P.; Goettel, J. T.; Mercier, H. P. A.; Sowlati-Hashjin, S.; Hazendonk, P.; Gerken, M. Chemistry - A European Journal 2015, 21, 6247-6256.
61. Dunning, T. H. Journal of Chemical Physics 1989, 90, 1007-1023.
62. Moller, C.; Plesset, M. S. Phys Rev 1934, 46, 0618-0622.
63. Peterson, K. A.; Figgen, D.; Goll, E.; Stoll, H.; Dolg, M. Journal of Chemical Physics 2003, 119, 11113-11123.
64. Becke, A. D. Journal of Chemical Physics 1993, 98, 5648-5652.
65. Lee, C. T.; Yang, W. T.; Parr, R. G. Phys Rev B 1988, 37, 785-789.

66. Raghavachari, K.; Trucks, G. W.; Pople, J. A.; Headgordon, M. Chem Phys Lett 1989, 157, 479-483.
67. Pople, J. A.; Head-Gordon, M.; Raghavachari, K. The Journal of Chemical Physics 1987, 87, 5968-5975.
68. Purvis, G. D.; Bartlett, R. J. The Journal of Chemical Physics 1982, 76, 1910-1918.
69. Pulay, P.; Fogarasi, G.; Pang, F.; Boggs, J. E. J Am Chem Soc 1979, 101, 2550-2560.
70. Nowak, M. J.; Lapinski, L.; Bienko, D. C.; Michalska, D. Spectrochim Acta A 1997, 53, 855-865.
71. Bienko, D. C.; Michalska, D.; Roszak, S.; Wojciechowski, W.; Nowak, M. J.; Lapinski, L. J Phys Chem A 1997, 101, 7834-7841.
72. L. Lapinski, M. J. N.
73. Van Duijneveldt, F. B.; Van Duijneveldt- van Derijdt, J. G. C. M.; Van Lenthe, J. H. Chem Rev 1994, 94, 1873-1885.
74. Boys, S. F.; Bernardi, F. Mol Phys 1970, 19, 553-&.
75. Frisch, M. J., Trucks, G. W. ; Schlegel, H. B.; Scuseria, G. E.; Robb, M. A.; Cheeseman, J. R.; Scalmani, G.; Barone, V.; Mennucci, B.; Petersson, G. A.; Nakatsuji, H.; Caricato, M.; Li, X.; Hratchian, H. P.; Izmaylov, A. F.; Bloino, J.; Zheng, G.; Sonnenberg, J. L.; Hada, M.; Ehara, M.; Toyota, K.; Fukuda, R.; Hasegawa, J.; Ishida, M.; Nakajima, T.; Honda, Y.; Kitao, O.; Nakai, H.; Vreven, T.; Montgomery, J. A., Jr.; Peralta, J. E.; Ogliaro, F.; Bearpark, M.; Heyd, J. J.; Brothers, E.; Kudin, K. N.; Staroverov, V. N.; Kobayashi, R.; Normand, J.; Raghavachari, K.; Rendell, A.; Burant, J. C.; Iyengar, S. S.; Tomasi, J.; Cossi, M.; Rega, N.; Millam, J. M.; Klene, M.; Knox, J. E.; Cross, J. B.; Bakken, V.; Adamo, C.; Jaramillo, J.; Gomperts, R.; Stratmann, R. E.; Yazyev, O.; Austin, A. J.; Cammi, R.; Pomelli, C.; Ochterski, J. W.; Martin, R. L.; Morokuma, K.; Zakrzewski, V. G.; Voth, G. A.; Salvador, P.; Dannenberg, J. J.; Dapprich, S.; Daniels, A. D.; Farkas, Ö.; Foresman, J. B.; Ortiz, J. V.; Cioslowski, J.; Fox. Wallingford CT, 2009.
76. Bulat, F. A.; Toro-Labbe, A.; Brinck, T.; Murray, J. S.; Politzer, P. J Mol Model 2010, 16, 1679-1691.
77. Lu, T.; Chen, F. Journal of Molecular Graphics and Modelling 2012, 38, 314-323.
78. Lu, T.; Chen, F. 2012, 33, 580-592.
79. Johnson, E. R.; Keinan, S.; Mori-Sánchez, P.; Contreras-García, J.; Cohen, A. J.; Yang, W. J Am Chem Soc 2010, 132, 6498-6506.
80. Keith, A. T.; TK Gristmill Software: Overland Park KS, USA, 2014.
81. Groom, C. R.; Bruno, I. J.; Lightfoot, M. P.; Ward, S. C. Acta Crystallogr B 2016, 72, 171-179.
82. Bader, R. F. W. Journal of Physical Chemistry A 1998, 102, 7314-7323.
83. Bader, R. Atoms In Molecules. A Quantum Theory; Clarendon Press: Oxford, 1990.
84. Cortés-Guzmán, F.; F.W. Bader, R. Complementarity of QTAIM and MO theory in the study of bonding in donor-acceptor complexes, 2005.
85. Del Bene, J. E.; Alkorta, I.; Elguero, J. Chem Phys Lett 2019, 721, 86-90.
86. Chaudhary, P.; Goettel, J. T.; Mercier, H. P.; Sowlati-Hashjin, S.; Hazendonk, P.; Gerken, M. Chemistry 2015, 21, 6247-6256.
87. Zierkiewicz, W.; Michalczyk, M.; Wysokinski, R.; Scheiner, S. J Mol Model 2019, 25, 152.
88. Shlykov, S. A.; Giricheva, N. I.; Titov, A. V.; Szwak, M.; Lentz, D.; Girichev, G. V. Dalton T 2010, 39, 3245-3255.

89. Dutton, J. L.; Sutrisno, A.; Schurko, R. W.; Ragogna, P. J. Dalton T 2008, 3470-3477.
90. Fleischer, H.; Schollmeyer, D. Acta Crystallogr E 2002, 58, o901-o903.
91. Williams, D. J.; Bevilacqua, V. L. H.; Morson, P. A.; Pennington, W. T.; Schimek, G. L.; Kawai, N. T. Inorg Chim Acta 2000, 308, 129-134.
92. Grabowski, S. J. Applied Organometallic Chemistry 2017, e3727.
93. Michalczyk, M.; Zierkiewicz, W.; Wysokiński, R.; Scheiner, S. Chemphyschem 2019, 20, 959-966.
94. Scilabra, P.; Terraneo, G.; Resnati, G. Acc Chem Res 2019, 52, 1313-1324.
95. Vogel, L.; Wonner, P.; Huber, S. M. Angew Chem Int Ed 2019, 58, 1880-1891.
96. Bortoli, M.; Ahmad, S. M.; Hamlin, T. A.; Bickelhaupt, F. M.; Orian, L. Phys Chem Chem Phys 2018, 20, 27592-27599.
97. Kříž, K.; Fanfrlík, J.; Lepšík, M. ChemPhysChem 2018, 19, 2540-2548.
98. Selvakumar, K.; Singh, H. B. Chem Sci 2018, 9, 7027-7042.
99. Alkorta, I.; Elguero, J.; Del Bene, J. E. ChemPhysChem 2018, 19, 1886-1894.
100. Gleiter, R.; Haberhauer, G.; Werz, D. B.; Rominger, F.; Bleiholder, C. Chem Rev 2018, 118, 2010-2041.
101. De Vleeschouwer, F.; Denayer, M.; Pinter, B.; Geerlings, P.; De Proft, F. J Comput Chem 2018, 39, 557-572.
102. Scheiner, S.; Lu, J. Chem Eur J 2018, 24, 8167-8177.
103. Nziko, V. d. P. N.; Scheiner, S. J Phys Chem A 2014, 118, 10849-10856.
104. Nziko, V. d. P. N.; Scheiner, S. J Org Chem 2015, 80, 2356-2363.
105. Nziko, V. d. P. N.; Scheiner, S. J Phys Chem A 2015, 119, 5889-5897.
106. Franconetti, A.; Quiñonero, D.; Frontera, A.; Resnati, G. Phys Chem Chem Phys 2019, 21, 11313-11319.
107. Scheiner, S. J Phys Chem A 2017, 121, 5561-5568.
108. Grabowski, S. J.; Sokalski, W. A. ChemPhysChem 2017, 18, 1569-1577.
109. Wysokiński, R.; Michalczyk, M.; Zierkiewicz, W.; Scheiner, S. Phys Chem Chem Phys 2019, 21, 10336-10346.
110. Zierkiewicz, W.; Michalczyk, M.; Scheiner, S. Phys Chem Chem Phys 2018, 20, 8832-8841.
111. Fanfrlík, J.; Zierkiewicz, W.; Švec, P.; Růžičková, Z.; Řezáč, J.; Michalczyk, M.; Růžička, A.; Michalska, D.; Hobza, P. J Mol Model 2017, 23, 328.
112. Dong, W.; Niu, B.; Liu, S.; Cheng, J.; Liu, S.; Li, Q. ChemPhysChem 2019, 20, 627-635.
113. Dong, W.; Wang, Y.; Cheng, J.; Yang, X.; Li, Q. Mol Phys 2019, 117, 251-259.
114. Xu, H.; Cheng, J.; Yang, X.; Liu, Z.; Li, W.; Li, Q. ChemPhysChem 2017, 18, 2442-2450.
115. Zierkiewicz, W.; Michalczyk, M.; Scheiner, S. Molecules 2018, 23, 1416.
116. Zhang, J.; Hu, Q.; Li, Q.; Scheiner, S.; Liu, S. Int J Quantum Chem 2019, 119, e25910.
117. Zierkiewicz, W.; Michalczyk, M.; Scheiner, S. Phys Chem Chem Phys 2018, 20, 4676-4687.

Table 1. Difference in electronic and Gibbs free energies (E_{el} and G, in kcal/mol) of $(H_3N)_2\cdots YF_4$ (Y = S, Se, Te, Po) of *trans* complex relative to the *cis* structure calculated at the MP2/aug-cc-pVDZ (I) level of theory.

	E_{el}	G
$(H_3N)_2\cdots SF_4$	5.56	9.38
$(H_3N)_2\cdots SeF_4$	0.02	-3.87
$(H_3N)_2\cdots TeF_4$	-5.21	-3.55
$(H_3N)_2\cdots PoF_4$	-5.02	-2.32

Table 2. Structural parameters (distances in Å, angles in degs) in *cis* $YF_4\cdot\cdot 2NH_3$ complexes at the MP2/aug-cc-pVDZ level.

	R(N···Y) R(N'···Y)	r(Y-F_e)	r(Y-F_a)	θ(F_e-Y-F_e)	θ(F_a-Y-F_a)	θ(N··Y··N)	R(H-F)[a]
$(H_3N)_2\cdots SF_4$	2.734 2.736	1.623 (+0.016)[b] 1.623 (+0.016)	1.741 (+0.037) 1.741 (+0.037)	95.1 (-6.3)	172.7 (+0.4)	112.9	2.981
$(H_3N)_2\cdots SeF_4$	2.683 2.686	1.749 (+0.026) 1.749 (+0.026)	1.845 (+0.041) 1.845 (+0.045)	91.3 (-9.2)	171.1 (+1.9)	121.8	2.941
$(H_3N)_2\cdots TeF_4$	2.501 2.951	1.909 (+0.028) 1.923 (+0.042)	1.988 (+0.043) 1.992 (+0.047)	85.6 (-15.3)	162.8 (-0.4)	130.8	2.571
$(H_3N)_2\cdots PoF_4$	2.568 2.766	2.006 (+0.034) 2.031 (+0.059)	2.101 (+0.052) 2.102 (+0.053)	85.9 (-13.3)	165.3 (-2.9)	129.0	2.499

[a] shortest distance between H and F atoms.

[b] change from geometry of isolated monomer in parentheses.

Table 3. Structural parameters (distances in Å, angles in degrees) in *trans* $YF_4 \cdot\cdot 2NH_3$ complexes at the MP2/aug-cc-pVDZ level.

	R(N···Y)	r(Y-F)	Σ θ (F-Y-F)	θ (N···Y···N)
$(H_3N)_2 \cdots SF_4$	1.872 3.126	1.762 1.762 1.775 1.775	354.3	140.2
$(H_3N)_2 \cdots SeF_4$	2.001 3.038	1.856 1.856 1.858 1.858	351.6	137.9
$(H_3N)_2 \cdots TeF_4$	2.197 3.038	1.984 1.984 1.988 1.988	345.5	129.4
$(H_3N)_2 \cdots PoF_4$	2.279 2.812	2.081 2.082 2.091 2.092	345.7	133.9

Table 4. Binding (E_b) and interaction (E_{int}) energies corrected for BSSE (kcal mol^{-1}) of YF_4 complexes with 2 NH_3 calculated at the MP2/ aug-cc-pVDZ (I), BLYP-D3/Def2TZVPP (II) and CCSD(T)/ aug-cc-pVDZ (III) levels of theory.

	E_b				E_{int}		
	(I)	(II)	(III)		(I)	(II)	(III)
cis							
$(H_3N)_2 \cdots SF_4$	-11.21	-12.96	-10.53		-13.10	-15.85	-12.33
$(H_3N)_2 \cdots SeF_4$	-17.16	-21.59	-16.07		-20.15	-25.30	-19.01
$(H_3N)_2 \cdots TeF_4$	-22.62	-25.40	-21.47		-28.82	-28.92	-27.77
$(H_3N)_2 \cdots PoF_4$	-32.37	-35.31	-31.24		-37.17	-40.58	-36.25
trans							
$(H_3N)_2 \cdots SF_4$	-2.76	-1.51	0.71		-50.40	-40.25	-47.50
$(H_3N)_2 \cdots SeF_4$	-14.42	-17.26	-11.81		-48.33	-45.97	-47.25
$(H_3N)_2 \cdots TeF_4$	-25.70	-26.30	-24.08		-46.27	-44.21	-45.99
$(H_3N)_2 \cdots PoF_4$	-34.90	-34.77	-33.60		-52.82	-51.23	-52.48

Table 5. Changes of selected harmonic frequencies (cm^{-1}) and infrared intensities (km/mol)[a] caused by complexations, calculated for *cis* complexes at MP2/aug-cc-pVDZ level of theory.

	S	Se	Te	Po	Assignment[b]
1	-45 (85.7)	-50 (62.5)	-46 (43.1)	-54 (51.7)	ν_s(Y-F_e)
2	-50 (108.1)	-60 (70.4)	-71 (50.8)	-71 (46.8)	ν_a(Y-F_e)
3	-57 (6.4)	-58 (59.1)	-43 (-9)	-71 (-97.7)	ν_a(Y-F_a)
4	-36 (-1.3)	-42 (0)	-53 (4.9)	-48 (17.7)	ν_s(Y-F_a)

[a] IR intensities in parentheses.
[b]Assignment from PED calculations. The predominant components of the PED matrix or their linear combination (e.g., stretching or bending).
Abbreviations: ν_s, symmetric stretching; ν_a, antisymmetric stretching.

Table 6. Changes of selected harmonic frequencies (cm^{-1}) and infrared intensities (km/mol)[a] caused by complexations, calculated for *trans* complexes at MP2/aug-cc-pVDZ level of theory.

	S	Se	Te	Po	Assignment [b]
1	-177 (-18.2)	-140 (-29.6)	-112 (-26.2)	-100 (-26)	ν_s(Y-F)
2	-205 (276.9)	-160 (214.6)	-129 (159)	-125 (153.7)	ν_a(Y-F)
3	-128 (-177.9)	-81 (-34.8)	-64 (-1.6)	-47 (-16.8)	ν_a(Y-F)
4	-88 (-2.6)	-82 (-1.5)	-71 (0.4)	-66 (16.7)	ν_s(Y-F)

[a] IR intensities in brackets.
[b]Assignment from PED calculations.

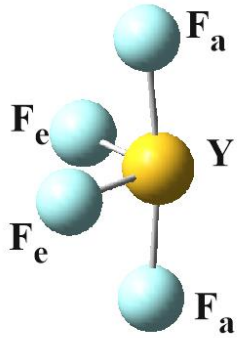

Fig. 1. Optimized structure of isolated YF_4 (Y = S, Se, Te, Po) monomers.

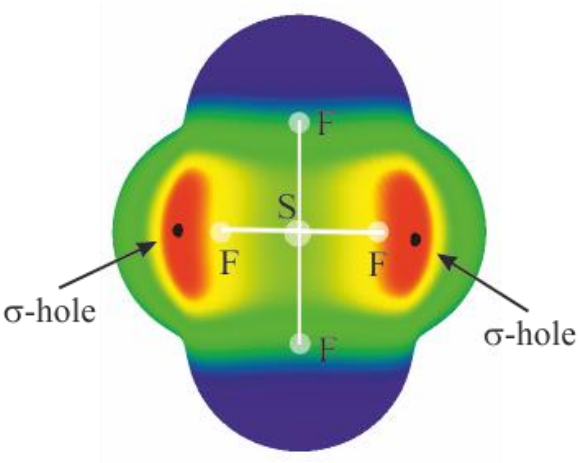

Fig. 2 MEP (on the 0.001 a.u. isodensity surface at the MP2/aug-cc-pVDZ level) of SF_4. Colour ranges, in kcal/mol, are: red greater than 30, yellow between 20 and 30, green between 0 and 20, blue below 0 kcal/mol

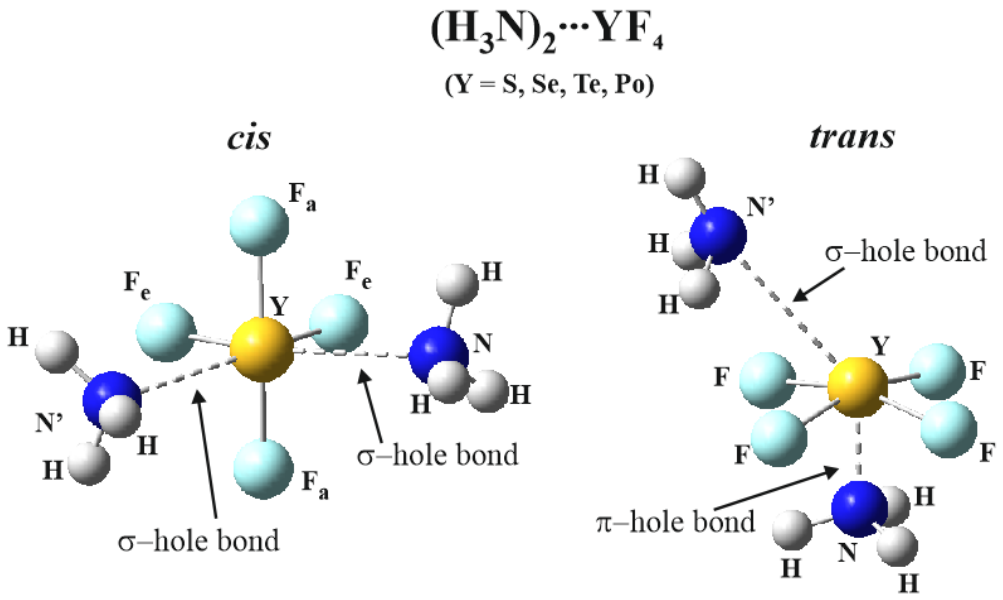

Fig 3. Structures of YF_4 complexes with two NH_3 molecules. N located closer to Y is labeled as N, and N' refers to the more distant one.

Fig. 4. AIM molecular diagrams showing the bond critical points (green dots) in *cis* and *trans* YF_4 complexes with 2 NH_3. Numbers located near green dots indicate the electron densities (ρ) at BCPs (in au). Data calculated at the MP2/aug-cc-pVDZ level.

	cis	*trans*
$(H_3N)_2\cdots SF_4$	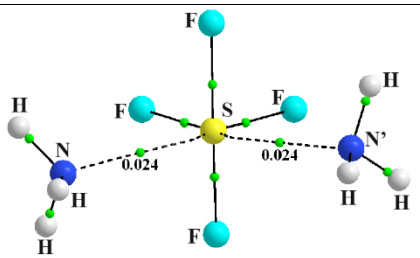	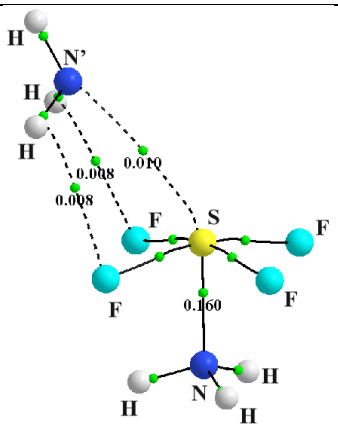

$(H_3N)_2\cdots SeF_4$	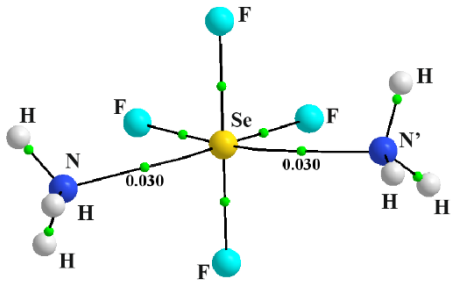	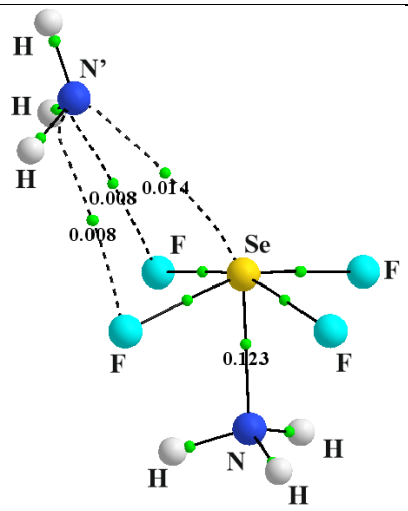
$(H_3N)_2\cdots TeF_4$	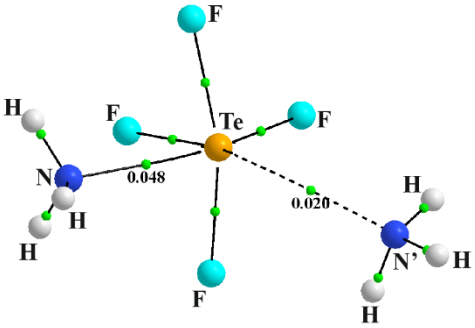	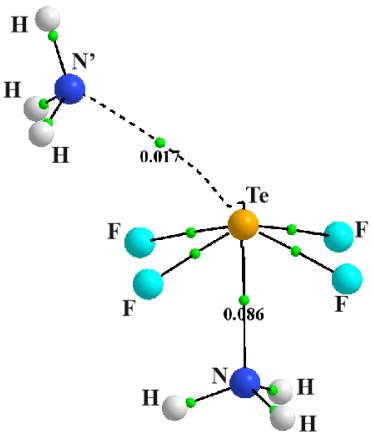
$(H_3N)_2\cdots PoF_4$	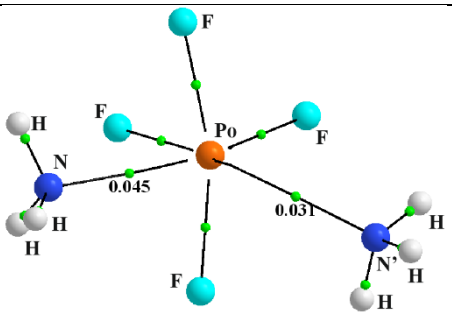	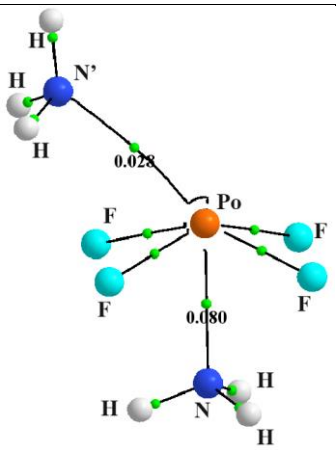

Fig 5. Crystal structures of illustrative examples of hexacoordinated Te atoms within complexes with various organic ligands. CSD Code provided on the right along with salient interatomic distances.

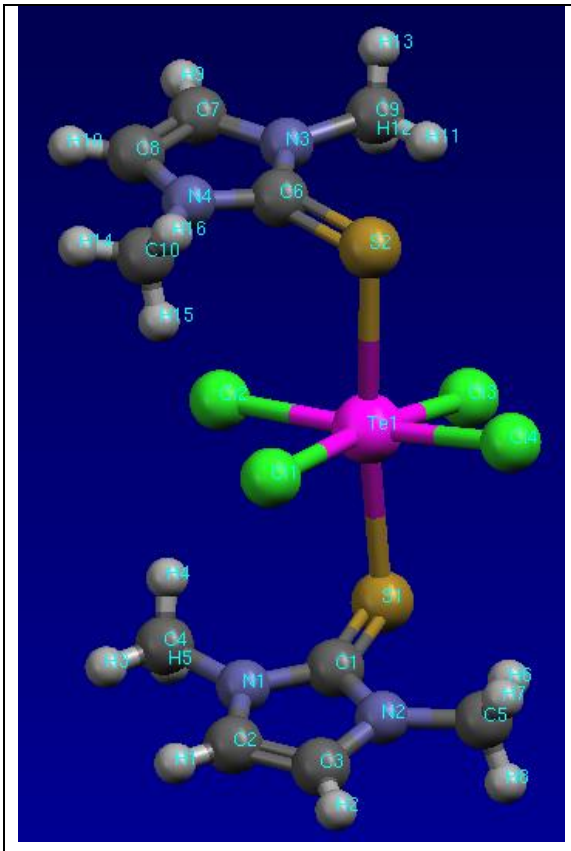	HUCCEN R(Te···S)= 2.588 Å R(Te···S)= 2.824 Å

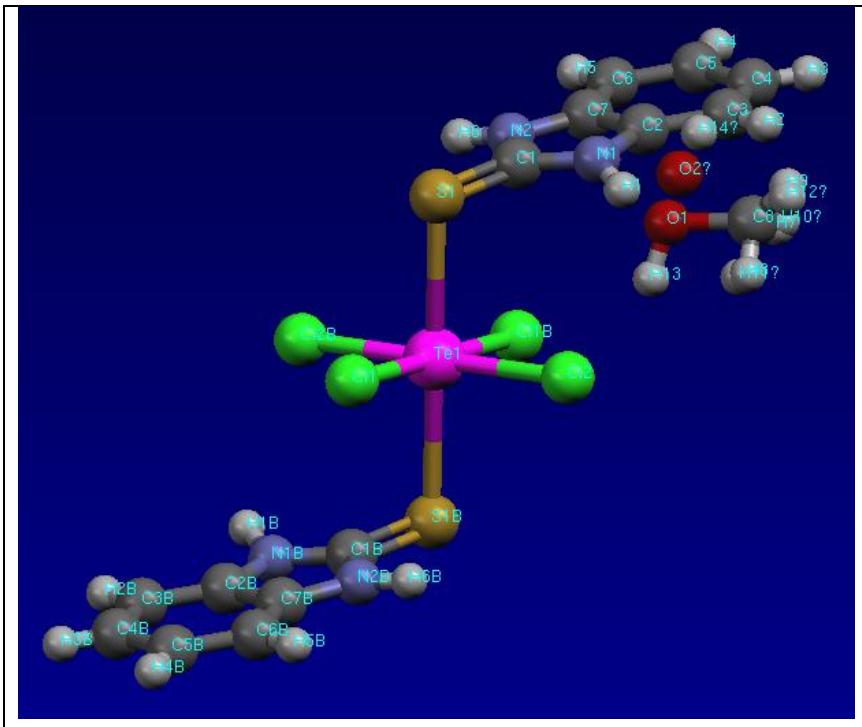	LUDJUP R(Te···S)= 2.696 Å R(Te···S)= 2.696 Å
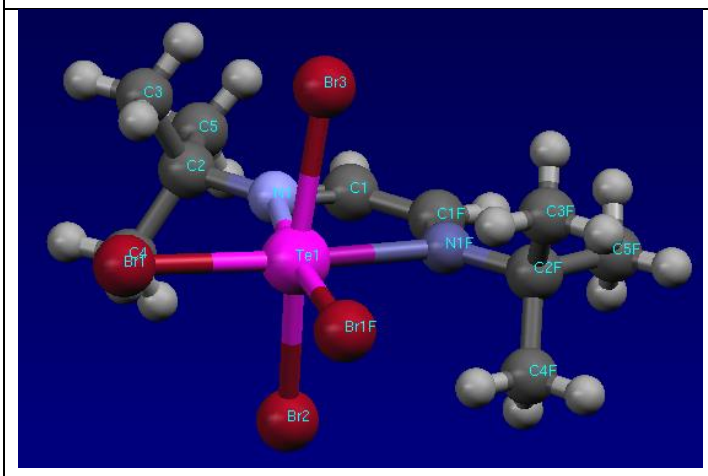	EFIVUL R(Te···N)= 2.466 Å R(Te···N)= 2.466 Å

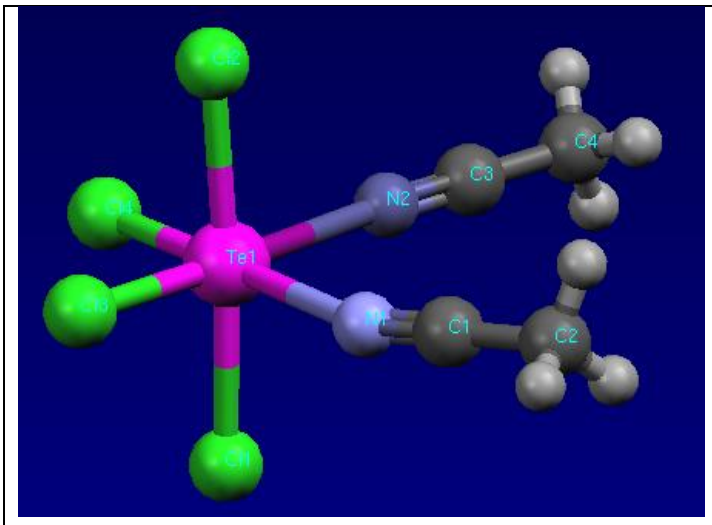	HUQNAJ R(Te···N)= 2.741 Å R(Te···N)= 2.752 Å